Grant agreement no. 243964

QWeCI

Quantifying Weather and Climate Impacts on Health in Developing Countries

Deliverable 3.2.a – Preliminary assessment of the characteristics of interannual variations of the intraseasonal variability of African temperature and precipitation in dynamical models and observations

Start date of project: 1st February 2010 Duration: 42 months

Lead contractor: IC3
Coordinator of deliverable: IC3
Evolution of deliverable

Due date : M24
Date of first draft : 18 April 2012
Start of review : 21 May 2012
Deliverable accepted : 24 May 2012

Project co-funded by the European Commission within the Seventh Framework Programme (2007-2013)		
Dissemination Level		
PU	Public	
PP	Restricted to other programme participants (including the Commission Services)	
RE	Restricted to a group specified by the consortium (including the Commission Services)	**RE**
CO	Confidential, only for members of the consortium (including the Commission Services)	

Preliminary assessment of the characteristics of interannual variations of the intraseasonal variability of African temperature and precipitation in dynamical models and observations

J. García-Serrano, I. Andreu-Burillo, O. Mula-Valls, F.J. Doblas-Reyes

The main task of this Deliverable is the validation of intraseasonal variability and the assessment of its forecast quality in the current operational version of the European Centre for Medium-range Weather Forecasts (ECMWF) seasonal prediction system. The work will be later extended to illustrate the performance of the National Centers for Environmental Prediction (NCEP) Climate Forecast System.

1. Introduction

Climate prediction is motivated by the evidence that current global climate models (GCMs) can, to a certain degree, capture the evolution of slow variations of the climate system when they are adequately initialised. In particular, the thermal inertia and assumed predictability of the sea surface temperatures (SSTs) imply that reliable seasonal predictions in the tropics are a realizable aim (Tompkins and Feudale 2010). The objective of this research is to evaluate the skill of the rainfall and temperature seasonal predictions, and the limit of its lead time, over western and southern Africa according to the countries where the pilot studies of QWeCI take place: Senegal, Ghana, and Malawi.

The tropical Atlantic rainfall variability over Africa is largely dominated by, and seasonally locked to, the summertime West African monsoon (WAM), which is tightly controlled by the inter-tropical convergence zone (ITCZ) latitudinal variability and the distribution of trade winds. The WAM is sensitive to both local forcing and remote influences (e.g. Folland et al. 1986; Fontaine and Janicot 1996; Fontaine et al. 1998). The WAM variability spans a wide range of timescales, from intraseasonal (e.g. Sultan et al. 2003) to interdecadal (e.g. Janicot et al. 2001). The interannual variability of the WAM is represented by changes in precipitation over coastal regions of the Gulf of Guinea, for which the Equatorial Atlantic SST variability or Atlantic Niño is the main oceanic forcing (Janicot et al. 1998, Vizy and Cook 2001; Okumura and Xie 2004; Losada et al. 2010). The decadal variability of the WAM is well captured by low-frequency rainfall fluctuations over the semi-arid African Sahel, the southern edge of the Sahara (Folland et al. 1986; Nicholson 1993; Fontaine et al. 1995). The Sahelian rainfall variability is related to contrasting patterns of SST anomalies on a near-global scale, projecting onto an inter-hemispheric signature (Folland et al. 1986; Palmer 1986; Rowell et al. 1995; Fontaine et al. 1998). As part of this inter-hemispheric SST pattern, the main oceanic forcings of the Sahel precipitation are the Indian Ocean decadal variability (Giannini et al. 2003, 2005; Bader and Latif 2003), the Atlantic multi-decadal oscillation, or AMO (Hoerling et al. 2006; Mohino et al. 2011), and the Pacific decadal oscillation or the basin-wide inter-decadal Pacific oscillation, or IPO (Joly 2008; Mohino et al. 2011).

The austral summer rains of southern Africa are also known to be sensitive to the state of global SSTs via a range of factors, many of them posing challenges for climate prediction (Reason et al. 2006). Some of this variability is thought to be forced remotely by El Niño-Southern Oscilation (ENSO) in the tropical Pacific. Some of the most severe droughts over subtropical southern Africa seem to be indeed due to strong ENSO events (Mason and Jury 1997; Reason et al. 2000). ENSO is known to project strongly over southern Africa and the South Atlantic, and tends to suppress (enhance) rainfall during the mature phase of warm (cold) events. This arises from changes in the regional atmospheric circulation, via modifications of the local Walker circulation (Reason et al. 2000), the South Indian Ocean convergence zone (Cook 2000, 2001) and the wavetrain response crossing the Southern Pacific basin (the Pacific-South America pattern; Mo and Peagle 2001). Another part of the African climate variability and associated extreme events is related to regional SST anomalies over the South Atlantic (Tennant and Reason 2005; Mason 1990, 1995). The most

prominent interdecadal South Atlantic mode, impacting significantly on both temperature and rainfall, is the Benguela Niño (Florenchie et al. 2003, 2004), which tends to be associated with changes in the trade winds. It has also been suggested that the tropical Indian Ocean variability plays a role in the southern African climate. The association between SSTs in the equatorial Indian basin and seasonal rainfall over South Africa is non-linear (Mason and Jury 1997). It should be emphasized that the SST variability in the South Indian Ocean has been believed to exert more influence over southern Africa than the South Atlantic SST variability (e.g. Mason and Jury 1997, Reason 2002) since the air masses originating over the former tend to be relatively warm and moist whereas those from the eastern Atlantic are relatively cool and dry. However, it has to be borne in mind that the climate impact of the South Atlantic Ocean on southern Africa are less well understood (Reason et al. 2006).

The WAM is a complex system with three main interacting components, namely atmosphere, land and ocean, whose different inertias generate complex interactions. A clear example is the latitudinal jump of the ITCZ-related rainbelt, whereby the Sahelian rainy season occurs in July-September and varies in intensity both at interannual and decadal timescales (e.g. Fontaine et al. 1998; Janicot et al. 1998; Sultan and Janicot 2000). The physical mechanisms driving WAM dynamics have been the subject of numerous diagnostics studies during the recent decades. However, prediction of the seasonal rainfall over West Africa still remains one of the major concern for the local population, because of its impact on agriculture, health and water supply, and consequently on the economy of its integrating countries. One of the objectives of this Deliverable aims to assess the maximum lead time, up to date, to forecast the WAM rainfall at intraseasonal-to-annual range in current seasonal prediction systems.

The Guinean precipitation and the Sahelian rainfall account for most of the SST-forced WAM variability at seasonal-to-decadal timescales. When climate models are forced with observed SSTs, they successfully reproduce the observed interannual-Guinean and decadal-Sahelian rainfall variabilities (Giannini et al. 2003, 2005; Moron et al. 2003; Tippet and Giannini 2006). Thus, the SST forcing can be considered as the dominant driver of the WAM rainfall variability. However, the WAM forecast skill in coupled models becomes a serious trouble. This is particularly true for predicting the interannual-to-decadal variability (Joly et al. 2007; Joly and Voldoire 2009a, 2009b; García-Serrano et al. 2012). Nonetheless, Batté and Déqué (2011), by using the ENSEMBLES Stream-2 seasonal re-forecasts, pointed out the additional skill in GCMs when compared to climatology for a variable highly dependent on parameterizations such as precipitation. These results are encouraging and contrast with the reputation coupled forecast systems have been given over the years when it comes to precipitation forecasts outside the tropical Pacific basin. Unfortunately, this does not translate into skill in predicting the dominant WAM rainfall regimes. Perhaps, the exception is the Guinean precipitation, for which there exists a maximum (up to date) forecast correlation with the observations of ~0.5-0.6 using direct model output of rainfall. The Sahelian precipitation, instead, remains a clear hurdle for coupled GCMs. Bouali et al. (2008), by using the DEMETER seasonal re-forecasts, found a correlation of 0.16 with raw rainfall data, while the model-output-statistics (MOS) calibration with atmospheric dynamics and moist static energy fluxes did not lead to better results. Maybe as evidence of the improvement in both models and ocean analysis, the skill at predicting summer monsoon rainfall anomalies has increased a bit in recent years. Thus, Philippon et al. (2010), by using the ENSEMBLES Stream-1 seasonal re-forecasts, improved the Sahelian forecasting from a correlation of 0.17 with direct model output of rainfall to 0.51 with MOS calibration, which included five atmospheric fields. Likewise, and in an operational seasonal prediction context, Tompkins and Feudale (2010) found a forecast correlation of the Sahelian rainfall of around ~0.4 using the ECMWF System3 re-forecasts. This Deliverable updates the skill and reproducibility of the dominant WAM rainfall regimes (Guinean and Sahelian) by evaluating the most recent operational seasonal prediction system at ECMWF, namely the ECMWF System4 (hereafter SYST4). In particular, one of the tasks of this Deliverable tackles an

innovative approach based on the assessment of the ability of these forecast systems in simulating and predicting the timing of the latitudinal migration of the tropical convection.

2. Seasonal re-forecasts

This Deliverable assesses the most recent seasonal-to-interannual operational climate forecast system developed at the European Centre for Medium-Range Weather Forecasts (ECMWF), the ECMWF System4[1]. In particular, the project will analyze sets of retrospective forecasts (re-forecasts or hindcasts) over a recent period produced by SYST4. The SYST4 re-forecasts have 15 members for all start dates (Feb, May, Aug, Nov), and cover the 30 years from 1981 to 2010; the length of these integrations is thirteen months. The long time period in the hindcasts allows reliable calibration of the forecasts and good assessment of their skill.

Standard analyses for the previous version of the ECMWF seasonal forecast system (ECMWF System3) have shown that the forecast quality for Pacific equatorial SSTs (i.e. ENSO) was substantially improved in comparison with previous ECMWF systems (Stockdale et al. 2011). Changes in skill for atmospheric variables were less clear. Overall, improvements in predictive skill were expected to be more evident during the Northern Hemisphere summer season, and in tropical regions throughout the year. Anderson et al. (2007) offer full details of the ECMWF System3.

3. Results

3.1. Seasonal forecast quality

Precipitation and air temperature seasonal forecast quality has been estimated using the correlation between the ensemble-mean predicted anomalies and the corresponding observation anomalies. The correlations were calculated for forecast times ranging from one to twelve months using the four start dates for which annual outlooks are available from the SYST4, i.e. those started on the first of February, May, August and November. The period over which the correlations were calculated was 1981-2010.

The precipitation observations used to calculate the correlations consisted of the Global Precipitation Climatology Project (GPCP) data set (Adler *et al.*, 2003). This comports monthly precipitation data on a 2.5°x2.5° latitude-longitude (Cylindrical Equal Distance) global array of points. The air temperature observations came from a combination of two data sets: over land, the Global Historical Climatology Network version 1.4.3 (GHCN; Peterson and Vose, 1997), with a latitude-longitude resolution of 0.5°; over the ocean, the Extended Reconstructed Sea Surface Temperature (ERSST) version 3.b (Smith *et al.*, 2008). This data set consists of monthly SST anomalies arranged in 5° grid boxes.

The climatologies of each forecast ensemble member and those corresponding to the observations were computed separately. Then, the corresponding anomalies were calculated by subtracting those climatologies from their respective full fields. For the predicted ensemble, this ensured that the anomalies of each member would be fully accounted for. Finally, the ensemble-mean of the forecast anomalies was computed.

Precipitation presents a strong decay in skill between forecast months one and two, regardless of the start date. The strength of the signal seems to step down again between forecast months four and five. However, there remain patches of skill that typically lie between 0.6 and 0.8 from October to January in the Indian Ocean. This coincides with the period of transition between the Northeast and

1 http://www.ecmwf.int/products/changes/system4/

the Southwest Monsoon. This behaviour is obvious for the start dates of May and August, for forecast dates less than ten months. After that forecast time, the skill is residual. In the Tropical Atlantic, between 10°S and 10°N, skill seems to concentrate around forecast times one to four months. Between these forecast times, the correlation can reach values within the (0.6,1.0) interval. However, the skill drops in October until February, for the start date of August. This region shows a latitudinal variation with time in the positioning of the patches with and without skill. The start date of November presents general good results. This positive skill could be due to ENSO and its impact on the entire tropical region. The Sahel shows a good forecast quality during the wet season of the West African Monsoon (WAM), between June and September (depending on the start date, even stretching into November), as well as the land around the Gulf of Guinea. The coherence of the skill signal is more important than the value it takes, which typically lies below 0.6.

The skill decay with forecast time appears to be slower for temperature than for precipitation, especially over sea areas, where the skill presents strong persistence. The higher skill for longer forecast times over the ocean might be due to the larger thermal inertia of the oceans, although it could be partly due to the coarser resolution of the SST observational data set used over ocean, which could be retaining longer time scales than the observations over land, the latter lying on a grid that is two orders of magnitude finer than the ERSST grid. The data set characteristics could be thereby amplifying the natural response-time differences between land and ocean. The oceanic region presenting the highest skill persistence is that of the Western Indian Ocean and the South Arabian Sea. The Atlantic Ocean presents higher skill variability, with recurring disappearance of skill (blue patch) south of 10°S in September to November from forecast time five months. Another important feature is the low skill band between 10°S and the Equator between the months of March and May. Skill over land presents higher variability than over the ocean, including a stronger overall decay from the first forecast month to the second. There is a region inside the continent where the lack of skill is quasi-systematic: this is the region that shows as white in all the maps with forecast time one month, located between latitudes 10°S and 10°N and longitudes 20°E and 30°E. Part of this lack of skill might be due to the lack of observations in the region. Areas of prevailing low skill are the North of Africa (north of Sahel) between October and May, with the highest incidence in March, and the Sahel region between June and October, which could be associated to the WAM cycle. There also appears to be low skill in South Africa. This is found twice in June, October and November and only in one map for August.

The ensemble-mean correlation maps are available at http://qweci.ic3.cat/index.php.

3.2. Prediction skill of the intraseasonal evolution of precipitation

The skill and reproducibility of the latitudinal migration of the ITCZ is examined by means of Hovmöller diagrams, in which the precipitation is longitudinally averaged as shown in Fig. 1 for West Africa (10ºW-10ºE) and South Africa (30ºE-40ºE), separately. Also shown in Fig. 1 is the spatial distribution of precipitation climatology in GPCP, which corresponds to the observational reference dataset, during boreal (July-September; JAS) and austral (January-March; JFM) summertime, which are the main rainy seasons in those regions. JAS and JFM represent the central months in the corresponding latitude-time Hovmöller diagrams analyzed, which span: May throughout November for West Africa, and November throughout May for South Africa. The target period of study for the Hovmöller diagrams is 1982-2008. The latitudinal window of the Hovmöller diagram in each case is: EQ-20ºN for West Africa, and 5ºS-25ºS for South Africa.

Monthly precipitation anomalies in these latitude-time diagrams are obtained by subtracting the corresponding monthly climatology. In that way, each month in the time dimension of the Hovmöller diagram involves interannual variability. Note that neither detrending nor filter has been applied to the data. After, a principal component analysis (PCA/EOF; von Storch and Zwiers 2001)

is performed upon these longitudinally-averaged precipitation anomalies. In this case, PCA provides a set of latitude-time patterns (empirical orthogonal functions, EOFs) and associated standardized time series (principal components, PCs). The information associated with each PCA mode is completed by the corresponding fraction of explained variance. The PCA results are also presented in terms of correlation maps, obtained by correlating the anomaly time series for surface temperature in different seasons with the PC related to each mode. Note that according to this PCA set-up, the leading EOFs correspond to the dominant interannual variability modes of the intra-seasonal evolution of precipiation.

The analysis first considers the West African monsoon. The systematic error of SYST4 in tropical convection is tightly associated with the warming drift in the tropical Atlantic SSTs (4ºS-4ºN / 15ºW-10ºE; Fig. 2, top right), which is a well-known problem in coupled GCMs leading to a southward shift of the local ITCZ and a failure to reproduce the Atlantic equatorial cold tongue (e.g. Richter and Xie 2008). Figure 2 shows how as the lead time for the Hovmöller diagram increases, that is when using predictions for the start dates from May to previous November, the SST warming drift in the boreal summer months is higher and, hence, rainfall biases are larger as well. The dipole-like pattern of the rainfall mean error reflects the wrong latitudinal position of the model ITCZ, which involves more rain than observed at equatorial latitudes and a clear deficit along the Sahelian belt (~10ºN-18ºN). Note also how SYST4 lengthens the WAM pre-onset stage, yielding a surplus of precipitation in July (one month later than observed).

The observed interannual variability of the longitudinally-averaged precipitation in West Africa is dominated by the Guinean (EOF1, 27%; Fig. 3) and Sahelian (EOF2, 20%; Fig. 4) rainfall regimes. The former reflects changes in convection strength within the ITCZ during the pre-onset months (first rainy season in the Gulf of Guinea; e.g. Fontaine et al. 2008), and is associated with the recent Atlantic-Pacific inter-tropical connection (e.g. Rodríguez-Fonseca et al. 2009). The latter shows a dipolar pattern with maximum amplitude over 10ºN-18ºN, which reflects more/less northward penetration of the rainbelt and projects onto the inter-hemispheric SST gradient (AMO, IPO). Note the AMO-related surface temperatures in the eastern Mediterranean basin and the positive correlations over the Saharan heat-low area during JAS, which have been shown to strongly contribute regulating the Sahelian precipitation (Haarsma et al. 2005; Biasutti et al. 2008; Fontaine et al. 2010).

The leading EOF mode of the longitudinally-averaged precipitation in SYST4 at each start date is the Guinean rainfall regime (Figs. 3,5), which accounts for 30%, 38%, and 39% of the total precipitation variance with predictions from the May, February, and November start dates, respectively. Notice that these fractions of variance in SYST4 overestimate that in GPCP. As the lead time for the Hovmöller diagram increases, successive EOF patterns reflect the model systematic error in tropical precipitation, where the Guinean precipitation increases in the model at the expense of the precipitation over the Sahel (cf. Figs. 3, 5 and Fig. 2). The Guinean precipitation modes capture the recent Atlantic-Pacific inter-tropical relationship. At each start date, the correlation maps of surface temperature suggest that SYST4 delays the peak of the Atlantic Niño with respect to the observations, occurring in JAS instead of MJ (Polo et al. 2008; Losada et al. 2010). This finding might be related to the systematic error described above (Fig. 2) on the model delay of the WAM pre-onset.

The second EOF of the longitudinally-averaged precipitation in SYST4 is the Sahelian rainfall regime (Figs. 4, 6), which accounts for 11%, 10%, and 10% of the total precipitation variance at the May, February, and November start dates, respectively. In this case, notice that these fractions of variance underestimate that in GPCP. For all start dates the simulated Sahelian mode shows a dipole-like pattern between the coastal regions and 10ºN-15ºN. As also shown in the observations, the heart of the simulated Sahelian rainfall occurs in August. The correlation maps of surface

temperature project onto the inter-hemispheric gradient that includes the AMO and IPO signatures, while no clear relationship appears with the Indian Ocean temperatures.

Ensemble-mean anomaly correlation coefficients between the longitudinally-averaged precipitation modes in GPCP and SYST4 show relevant results (Fig. 7). i) The Guinean rainfall (leading EOF) skill is statistically significant with a lead time of up to three months, with ~0.8 for the May start date (zero lead time) and ~0.5 for the February start date. The sharp decrease in the prediction skill of the Guinean rainfall (Fig. 7) appears to be consistent with the progressive lack of skill in forecasting the evolution of the cold tongue in the equatorial Atlantic as the lead time for May-June increases, as revealed in Section 3.1. This is also in agreement with the skill decay in forecasting precipitation anomalies over maritime regions of the Gulf of Guinea (Section 3.1).ii) The Sahelian mode (second EOF) has statistically significant skill only for the start date of May (zero lead time) with a correlation above 0.6, while for the February star date is ~0.45. Nevertheless, it is worth noting that SYST4 yield positive correlations for both Hovmöller-based rainfall modes at the three start dates considered. Especially noticeable is the score above 0.3 in the Sahelian precipitation for the November start date. Actually, the mild decrease in the prediction skill of the Sahelian rainfall (Fig. 7) could be consistent with the good performance in forecasting surface temperatures over the eastern Mediterranean basin and the Sahara heat low region during the target period July-to-September, as shown in Section 3.1. Likewise, these results seem to be in agreement with the positive correlations found for the Sudan-Sahel belt precipitation from the three start dates considered here (Section 3.1).

The other target area for the analysis of the interannual variability of the intraseasonal evolution of the precipitation is Southeastern Africa (see Fig. 1). The GPCP climatology of the Hovmöller diagram shows an evolution not as latitudinally-dependent (along the seven months considered) as in the case of the WAM, albeit a slight poleward excursion and intensification in January is noticeable (Fig. 8). This result likely suggests that latitude-time analysis of the longitudinally-averaged precipitation is not as appropriate for this region as for the WAM dynamics. SYST4 simulates reasonably well the precipitation over this area (Fig. 8), the systematic error only showing a progressive overestimation of the equatorial rainfall into late austral summer (5ºS-10ºS) and a weak poleward tendency in January (20ºS-25ºS).

The observed interannual variability of the longitudinally-averaged precipitation in Southeastern Africa (30ºE-40ºE) is dominated by changes at tropical latitudes early in autral summer (Nov-Dec) and at subtropical latitudes during late summer and early autumn (Feb-Apr). This first EOF accounts for 27% of the total variance; and it appears to be associated with significant SST anomalies in the subtropical latitudes of the Indian Ocean in early summer and a wave-like structure of SST anomalies along the Southern Ocean in late-summer (Fig. 9). Note also that this rainfall mode shows significant SST anomalies over the Benguela upwelling region in JFM. The second EOF (14%) is associated with the El Niño-Southern Oscillation (ENSO) in the Pacific Ocean. The latter appears to affect equatorial-tropical latitudes in Nov-Dec and tropical-subtropical latitudes during mid and late summer. The third dominant EOF (11%) shows a north-south dipolar structure centred in January, which appears to be associated (as the leading EOF) with a wave-like structure along the Southern Ocean in late summer (JFM).

ENSO dominates the variability of the longitudinally-averaged precipitation in Southeastern Africa for the three SYST4 start dates considered. The corresponding mode explains 17% of the variability in November, 16% in August, and 14% in May. Note that, in contrast to the West African case, the November start date is now the zero lead time prediction. However, the fraction of variance explained by ENSO is not so high compared with the rest of the leading modes. Actually the three first rainfall modes at each start date explain similar percentages of total variance ranging 10-15%, which again suggests that System 4 is not correctly reproducing the sources of prediction for

Southeastern Africa. This is further confirmed in the table below that shows cross-correlation analysis between the three observed EOF modes (Fig. 9) and the corresponding three leading modes from each start date. Substantial correlations are found only for the first start date (November), although the results are not particularly clear as both the leading and third SYST4 EOFs (Fig. 10) are correlated to the first and second observed patterns. This conclusion could be linked to the low prediction skill of precipitation found in South Africa at grid-point level (Section 3.1).

		SYST4								
		May			**Aug**			**Nov**		
		#1	#2	#3	#1	#2	#3	#1	#2	#3
GPCP	#1	0.19	-0.22	-0.24	0.14	-0.05	-0.14	0.43	-0.28	0.29
	#2	0.25	-0.22	-0.06	0.24	-0.02	0.09	0.41	0.20	0.53
	#3	-0.08	0.36	-0.05	0.01	-0.03	0.09	0.22	-0.13	0.08

4. Conclusions

This deliverable dealt with assessing the forecast quality of the SYST4 predictions of precipitation and surface air-temperature in West Africa and southeastern Africa. The main objective of the study was to evaluate the evolution of the skill of seasonal-to-annual predictions with lead time for the interannual variability of the African intraseasonal precipitation evolution. To this aim, the authors first assessed the grid-point ensemble-mean skill over the whole African continent and the ability of the forecast system in simulating and predicting the seasonal timing of the latitudinal migration of the deep tropical convection over two target regions.

The pointwise ensemble-mean skill plots showed a decay of the skill after forecast time four months for both precipitation and air temperature. However, due to the persistence of some of the climate processes affecting the continent, there are areas of skill persistence up to forecast month ten. In some of these areas, it is not the value that the skill takes, but the coherence in space and time that is most important.

The skill assessment of the longitudinally-averaged precipitation over West Africa (10ºW-10ºE) revealed levels of skill not achieved so far by using direct model output of rainfall. The Guinean precipitation regime, associated with anomalous convection in the ICTZ, reached correlations of about 0.8 at the start date of May (zero lead time) and 0.5 at the start date of February (3-month lead time). The Sahelian precipitation regime, associated with anomalous latitudinal displacements of the ITCZ, reached correlations of about 0.6 at the start date of May, 0.45 in February, and 0.3 at the start date of (the previous) November (6-month lead time). The same latitude-time, Hovmöller analysis but applied to Southeastern Africa (longitudinal-averaging window 30ºE-40ºE) did not yield encouraging results.

Acknowledgements
GPCP Precipitation data was provided by the NOAA/OAR/ESRL PSD, Boulder, Colorado, USA, from their Web site at http://www.esrl.noaa.gov/psd/. We would also like to acknowledge NOAA ESRL for the ERSST data.

References

Adler, R.F., G.J. Huffman, A. Chang, R. Ferraro, P. Xie, J. Janowiak, B. Rudolf, U. Schneider, S. Curtis, D. Bolvin, A. Gruber, J. Susskind, P. Arkin (2003): The Version 2 Global Precipitation Climatology Project (GPCP) Monthly Precipitation Analysis (1979-Present). *J. Hydrometeor.*, 4, 1147-1167.

Anderson, D., T. Stockdale, M. Balmaseda, L. Ferranti, F. Vitart, F. Molteni, F. J. Doblas-Reyes, K.

Mogenson, A. Vidard (2007): Development of the ECMWF seasonal forecast System 3. Tech. Memo. 503, ECMWF, www.ecmwf.int/publications/.

Bader, J., M. Latif (2003): The impact of decadal-scale Indian Ocean sea surface temperature anomalies on Sahelian rainfall and the North Atlantic Oscillation. *Geophys. Res. Lett.*, 30, 2169, doi 10.1029/2003GL018426.

Batté, L., M. Déqué (2011): Seasonal predictions of precipitation over Africa using coupled ocean-atmosphere general circulation models: skill of the ENSEMBLES project multimodel ensemble forecasts. *Tellus A*, 63.

Biasutti, M., I. M. Held, A. H. Sobel, A. Giannini (2008): SST forcings and Sahel rainfall variability in simulations of the twentieth and twenty-first centuries. *J. Clim.*, 21, 3471-3486.

Bouali, L., N. Philippon, B. Fontaine, J. Lemond (2008): Performance of DEMETER calibration for rainfall forecasting purposes: application to the July-August Sahelian rainfall. *J. Geophys. Res.*, 113, D15111.

Cook, K. H. (2000): The South Indian convergence zone and interannual rainfll variability over southern Africa. *J. Clim.*, 13, 3789-3804.

Cook, K. H. (2001): A Southern Hemispehre wave response to ENSO with implications for southern African precipitation. *J. Atmos. Sci.*, 58, 2146-2162.

Doblas-Reyes, F. J., A. Weisheimer, T. N. Palmer, J. M. Murphy, D. Smith (2010): Forecast quality assessment of the ENSEMBLES seasonal-to-decadal Stream 2 hindcasts. ECMWF Tech Memo 621, 45pp, Reading UK.

Florenchie, P., J. R. E. Lutjeharms, C. J. C. Reason, S. Masson, M. Rouault (2003): The source of Benguela Niños in the South Atlantic Ocean. *Geophys. Res. Lett.*, 30, 8009, doi:10.1029/2002GL014840.

Florenchie, P., C. J. C. Reason, J. R. E. Lutjeharms, M. Rouault, C. Roy (2004): Evolution of interannual warm and cold events in the southeast Atlantic ocean. *J. Clim.*, 17, 2318-2334.

Folland, C. K., T. N. Palmer, D. E. Parher (1986): Sahel rainfall and worldwide sea surface temperature. *Nature*, 320, 602-607.

Fontaine, B., S. Janicot, V. Moron (1995): Rainfall anomaly patterns and wind field signals over West Africa in August (1958-1989). *J. Clim.*, 8, 1503-1510.

Fontaine, B., S. Janicot (1996): Near-global sea surface temperature variability associated with West African rainfall anomaly types. *J. Clim.*, 9, 2935-2940.

Fontaine, B., S. Trzaska, S. Janicot (1998): Evolution of the relationship between near global and Atlantic SST modes and the rainy season in West Africa: statistical analyses and sensitivity experiments. *Clim. Dyn.*, 14, 353-368.

Fontaine, B., S. Louvet, P. Roucou (2008): Definition and predictability of an OLR-based West African monsoon onset. *Int. J. Climatol.*, 28, 1787-1798.

Fontaine, B., J. García-Serrano, P. Roucou, B. Rodríguez-Fonseca, T. Losada, F. Chauvin, S. Gervois, S. Sijikumar, P. Ruti, S. Janicot (2010): Impacts of warm and cold situations in the Mediterranean basins on the West African monsoon: observed connection patterns (1979-2006) and climate simulations. *Clim. Dyn.*, 35, 95-114.

García-Serrano, J., F. J. Doblas-Reyes, R. J. Haarsma, I. Polo (2012): Decadal prediction of the West African monsoon. *J. Geophys. Rev.* (under review).

Giannini, A., R. Saravanan, P. Chang (2003): Oceanic forcing of Sahel rainfall on interannual to interdecadal timescales. *Science*, 302, 1027-1030.

Giannini, A., R. Saravanan, P. Chang (2005): Dyamics of the boreal summer African monsoon in the NSIPP1 atmospheric model. *Clim. Dyn.*, 25, 517-535.

Haarsma, R. J., F. M. Selten, S. L. Weber, M. Kliphuis (2005): Sahel rainfall variability and response to greenhouse warming. *Geophys. Res. Lett.*, 32, L17702, doi:10.1029/2005GL023232.

Hoerling, M., J. Hurrell, J. Eischeid, A. Phillips (2006): Detection and attribution of twentieth-century Northern and Southern African rainfall change. *J. Clim.*, 19, 3989-4008.

Janicot, S., A. Harzallah, B. Fontaine, V. Moron (1998): West African monsoon dynamics and eastern equatorial Atlantic and Pacific SST anomalies. *J Clim.*, 11, 1874-1882.

Janicot, S., S. Trzaska, I. Poccard (2001): Summer Sahel-ENSO teleconnection and decadal time scale SST variations. *Clim. Dyn.*, 18, 303-320.

Joly, M., A. Voldoire, H. Douville, P. Terray, J.-F. Royer (2007): African monsoon teleconnections with tropical SSTs: validation and evolution in a set of IPCC4 simulations. *Clim. Dyn.*, 29, 1-20.

Joly, M (2008): Rôle des océans dans la variabilité climatique de la Mousson Africaine. PhD Dissertation, Université Paris-Est.

Joly, M., A. Voldoire (2009a): Influence of ENSO on the West African monsoon: temporal aspects and atmospheric processes. *J. Clim.*, 22, 3193-3210.

Joly, M., A. Voldoire (2009b): Role of the Gulf of Guinea in the inter-annual variability of the West African monsoon: what do we learn from CMIP3 coupled simulations?. *Int. J. Climatol.*, doi 10.1002/joc.2026.

Losada, T., B. Rodríguez-Fonseca, S. Janicot, S. Gervois, F. Chauvin, P. Ruti (2010): A multi-model approach to the Atlantic equatorial mode: impact on the West African monsoon. *Clim. Dyn.*, 35, 29-43.

Mason, S. J. (1990): Temporal variability of sea surface temperature around southern Africa. *J. Sci.*, 86, 243-252.

Mason, S. J. (1995): Sea-surface temperature-South African rainfall associations, 1910-1989. *Int. J. Climatol.*, 15, 119-135.

Mason, S. J., M. J. Jury (1997): Climate variability and change over spouthern Africa: a reflection on underlying processes. *Prog. Phys. Geog.*, 21, 23-50.

Mo, K. C., J. Paegle (2001): The Pacific-South America pattern and their downstream effects. *Int. J. Climatol.*, 21, 1211-1229.

Mohino, E., S. Janicot, J. Bader (2011): Sahelian rainfall and decadal to multidecadal SST variability. *Clim. Dyn.*, 37, 419-440.

Moron, V., N. Philippon, B. Fontaine (2003): Skill of Sahel rainfall variability in four atmospheric GCMs forced by prescribed SST. *Geophys. Res. Lett.*, 30, 2221, doi 10.1029/2003GL018006.

Nicholson, S. E. (1993): An overview of African rainfall fluctuations of the last decade. *J. Clim.*, 6, 1463-1466.

Okumura, Y., S.-P. Xie (2004): Interaction of the Atlantic equatorial cold tongue and the African monsoon. *J. Clim.*, 17, 3589-3602.

Palmer, T. N. (1986): Influence of the Atlantic, Pacific, and Indian oceans on Sahel rainfall. *Nature*, 322, 251-253.

Peterson, T. C., and R. S. Vose (1997): An overview of the Global Historical Climatology Network temperature database. Bull. Am. Met*eorol. Soc.*, 78, 2837-2849

Philippon, N., F. J. Doblas-Reyes, P. M. Ruti (2010): Skill, reproducibility and potential predictability of the West African monsoon in coupled GCMs. *Clim. Dyn.*, 35, 53-74.

Polo, I., B. Rodríguez-Fonseca, T. Losada, J. García-Serrano (2008): Tropical Atlantic Variability modes (1979-2001). Part I: time-evolving SST modes related to West African rainfall. *J. Clim.*, 21, 6457-6475.

Reason, C. J. C., R. J. Allan, J. A. Lindesay, T. J. Ansell (2000): ENSO and climatic signals across the Indian Ocean basin in the global context: Part I, interannual composite patterns. *Int. J. Climatol.*, 20, 1285-1327.

Reason, C. J. C. (2002): Sensitivity of the southern African circulation to dipole SST patterns in the South Indian Ocean. *Int. J.Climatol.*, 22, 377-393.

Reason, C. J. C., W. Landman, W. Tennant (2006): Seasonal to decadal prediction of southern African cliamte and its links with variability of the Atlatnic Ocean. *Bull. Amer. Meteor. Soc.*, 87, 941-955.

Richter, I., S.-P. Xie (2008): On the origin of the equatorial Atlantic biases in coupled general circulation models. *Clim. Dyn.*, 31, 587-598.

Rodríguez-Fonseca, B., I. Polo, J. García-Serrano, T. Losada, E. Mohino, C. R. Mechoso, F. Kucharski (2009): Are Atlantic Niños enhancing Pacific ENSO events in recent decadaes?. *Geophys. Res. Lett.*, 36, L20705, doi 10.1029/2009GL040048.

Rowell, D. P., C. K. Folland, K. Maskell, N. M. Ward (1995): Variability of summer rainfall over tropical North Africa (1906-92): observations and modelling. *Q. J. R. Meteorol. Soc.*, 121, 669-704.

Saha, S. and co-authors (2006): The NCEP Climate Forecast System. *J. Clim.*, 19, 3483-3517.

Saha, S. and co-authors (2011): The NCEP Climate Forecast System version 2. *J. Clim.* (to be submitted).

Smith, T. M., R. W. Reynolds, T. C. Peterson, J. Lawrimore (2008): Improvements to NOAA's historical merged land–ocean surface temperature analysis (1880–2006). *J. Clim.*, 21, 2283–2296.

Stockdale, T.N., D.L.T. Anderson, M.A. Balmaseda, F.J. Doblas-Reyes, L. Ferranti, K. Mogensen, T.N. Palmer, F. Molteni, F. Vitart (2011): ECMWF seasonal forecast System 3 and its prediction of sea surface temperature. *Clim. Dyn.*, 37, 455-471, doi:10.1007/s00382-010-0947-3.

Sultan, B., S. Janicot (2000): Abrupt shift of ITCZ over West Africa and intra-seasonal variability. *Geophys. Res. Lett.*, 27, 3353-3356.

Sultan, B., S. Janicot, A. Diedhiou (2003): The West African monsoon dynamics. Part I: documentation of intraseasonal variability. *J. Clim.*, 16, 3389-3406.

Tennant, W. J., C. J. C. Reason (2005): Associations between the global energy cycle and regional rainfall in South Africa and Southwest Australia. *J. Clim.*, 18, 3032-3047.

Tippet M. K., A. Giannini (2006): Potentially predictable components of African summer rainfall in an SST-forced GCM simulation. *J. Clim.*, 19, 3133-3144.

Tompkins, A. M., L. Feudale (2010): Seasonal ensemble predictions of West African monsoon precipitation in the ECMWF System 3 with a focus on the AMMA special observing period in 2006. *Wea. Forecasting*,

25, 768-788.

Vizy, E. K., K. H. Cook (2001): Mechanisms by which Gulf of Guinea and eastern North Atlantic sea surface temperature anomalies can influence African rainfall. *J. Clim.*, 14, 795-821.

von Storch, H., F. W. Zwiers (2001): Statistical analysis in climate research. Cambridge University Press, UK.

Yuan, X., E. F. Wood, L. Luo, M. Pan (2011): A first look at Climate Forecast System version 2. *Geophys. Res. Lett.*, 38, L13402, doi:10.1029/2011GL047792.

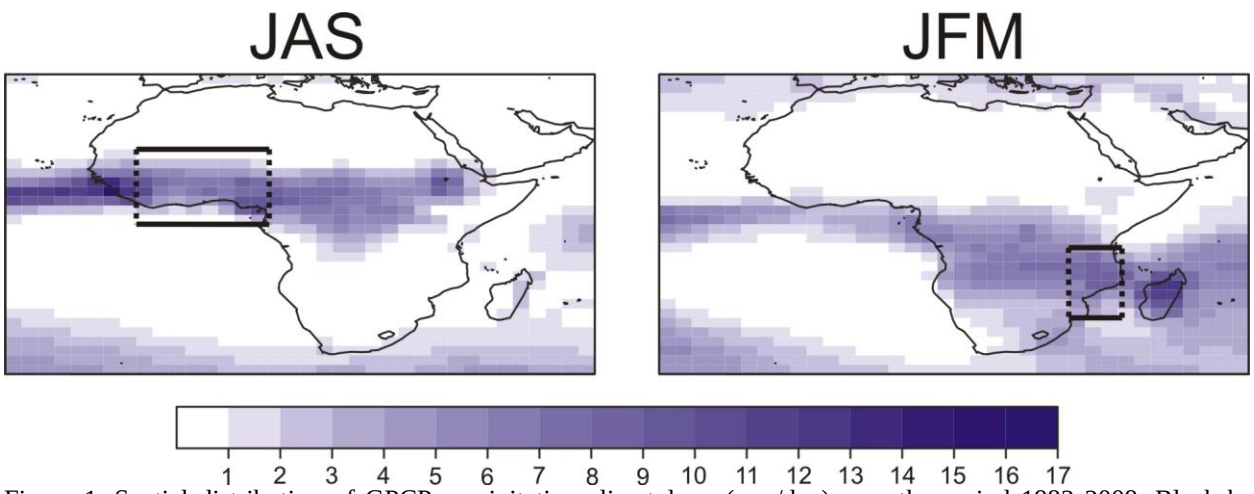

Figure 1. Spatial distribution of GPCP precipitation climatology (mm/day) over the period 1982-2008. Black boxes indicate the spatial domain for each case study: longitudinal-average along 10ºW-10ºE and latitudinal window over EQ-20ºN for West Africa in boreal summer (left); longitudinal-average along 30ºE-40ºE and latitudinal window over 5ºS-25ºS for eastern South Africa in austral summer (right).

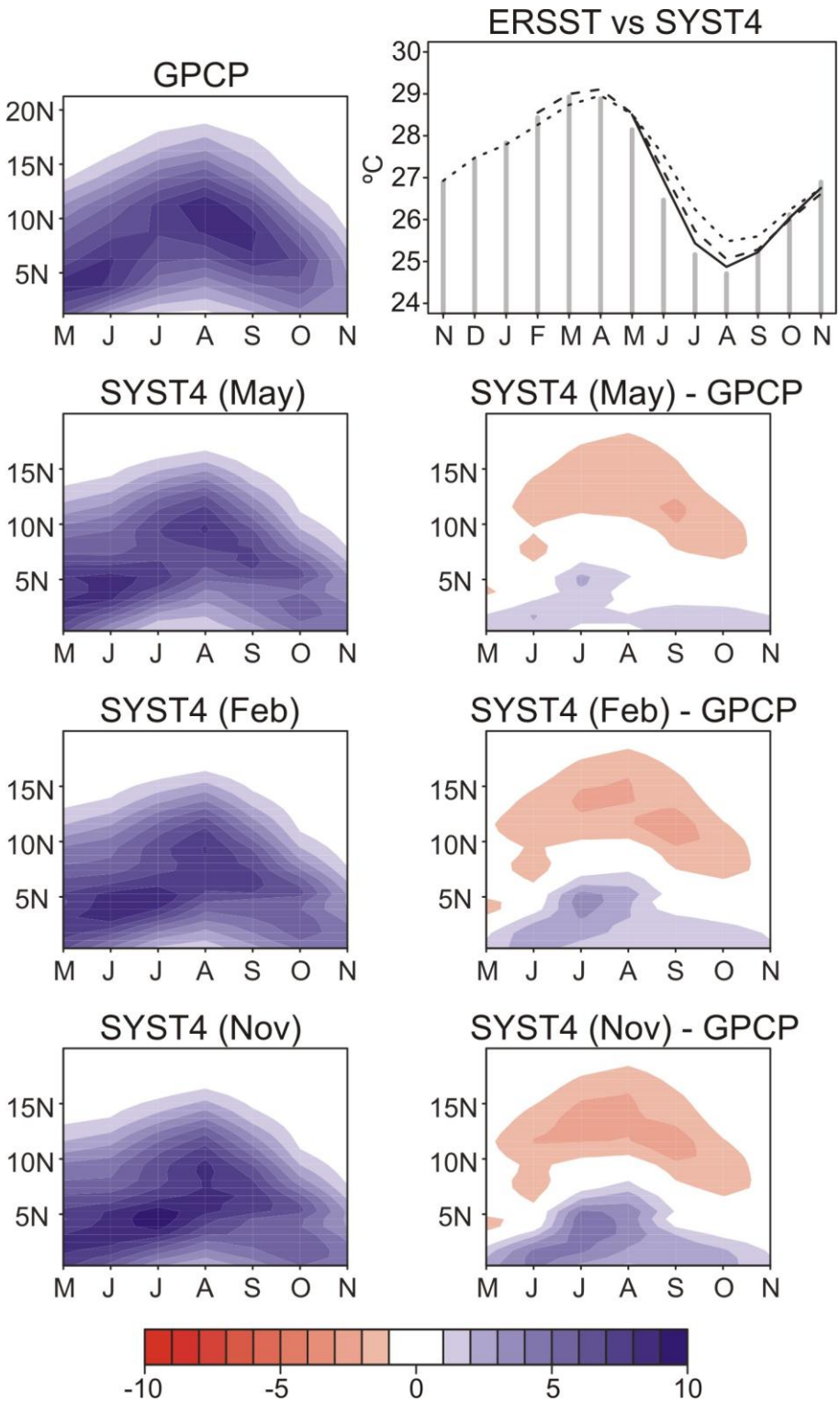

Figure 2. Hovmöller latitude-time diagrams of West African (see Fig. 1) precipitation climatology (mm/day) for GPCP (top-left) and ECMWF-System4 (left column), and the differences between them (right column). The seasonal cycle of the equatorial Atlantic SST averaged over 4ºS-4ºN / 15ºW-10ºE is also shown (top-right) for observations (grey bars) and the three start dates considered: May (zero lead time; solid black), February (3-month lead time; dashed black), and November (6-month lead time; dotted black). Period of study for the Hovmöller diagram is 1982-2008.

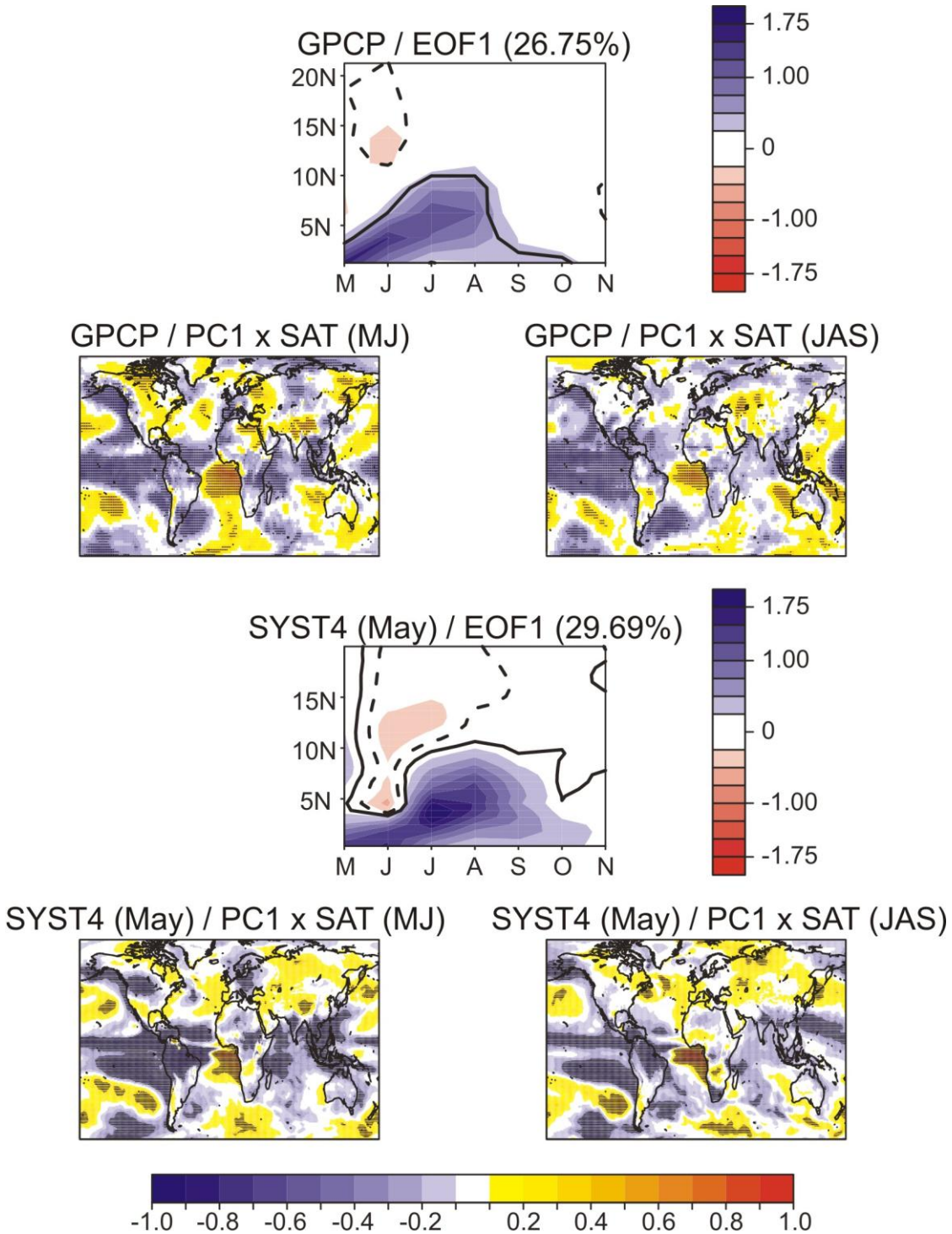

Figure 3. (top) Leading observational EOF of the longitudinally-averaged West African precipitation (10ºW-10ºE) over the period 1982-2008; and associated correlation maps of the principal component onto the surface air temperature (NCEP/NCAR) for boreal early-summer (May-June) and late-summer (July-September). (bottom) Same as (top) but upon the start date of May in the ECMWF-System4 seasonal/annual hindcasts. The principal component analysis applied to ECMWF-System4 was carried out by considering all the members in the co-variance matrix (Philippon et al. 2010).

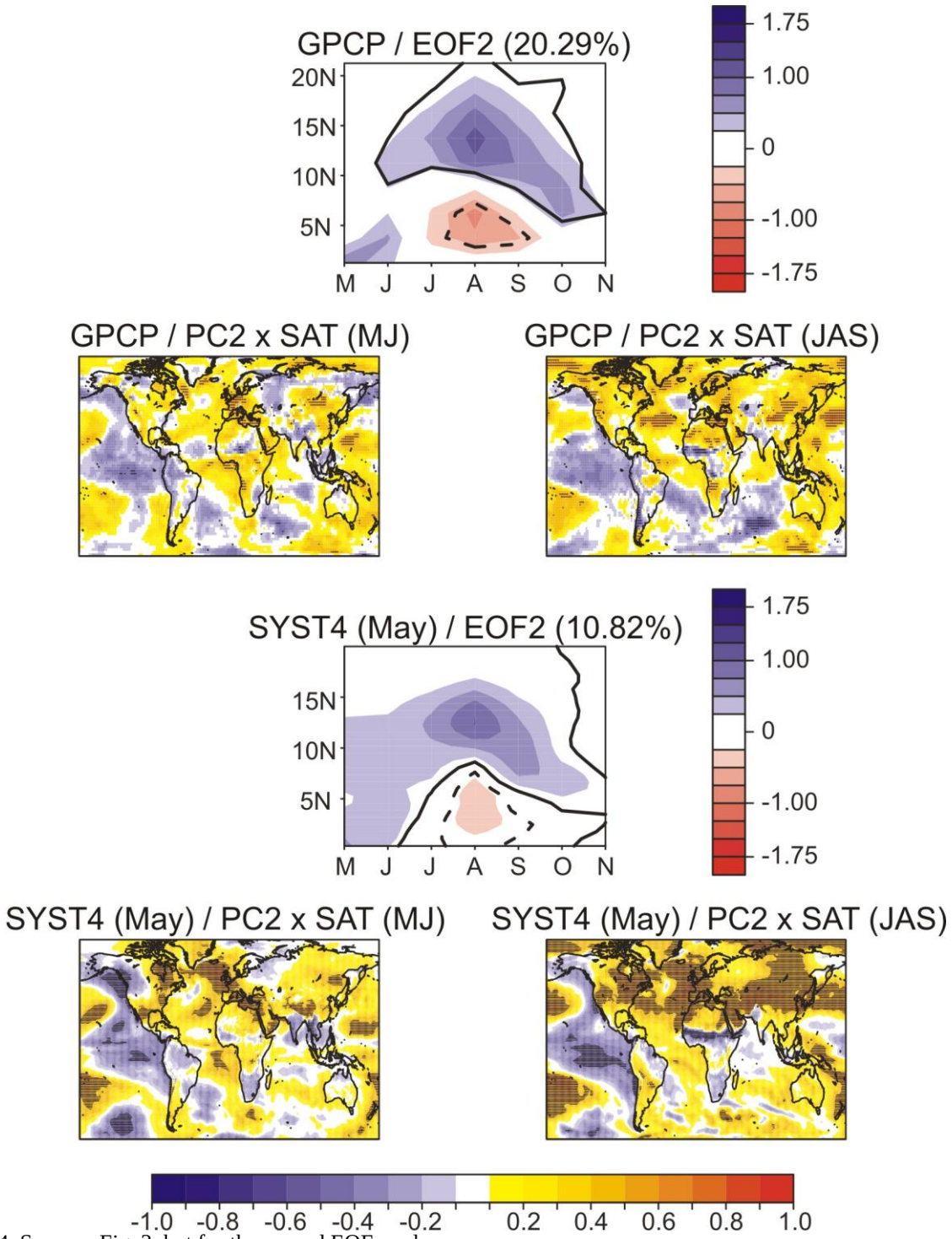

Figure 4. Same as Fig. 3, but for the second EOF mode.

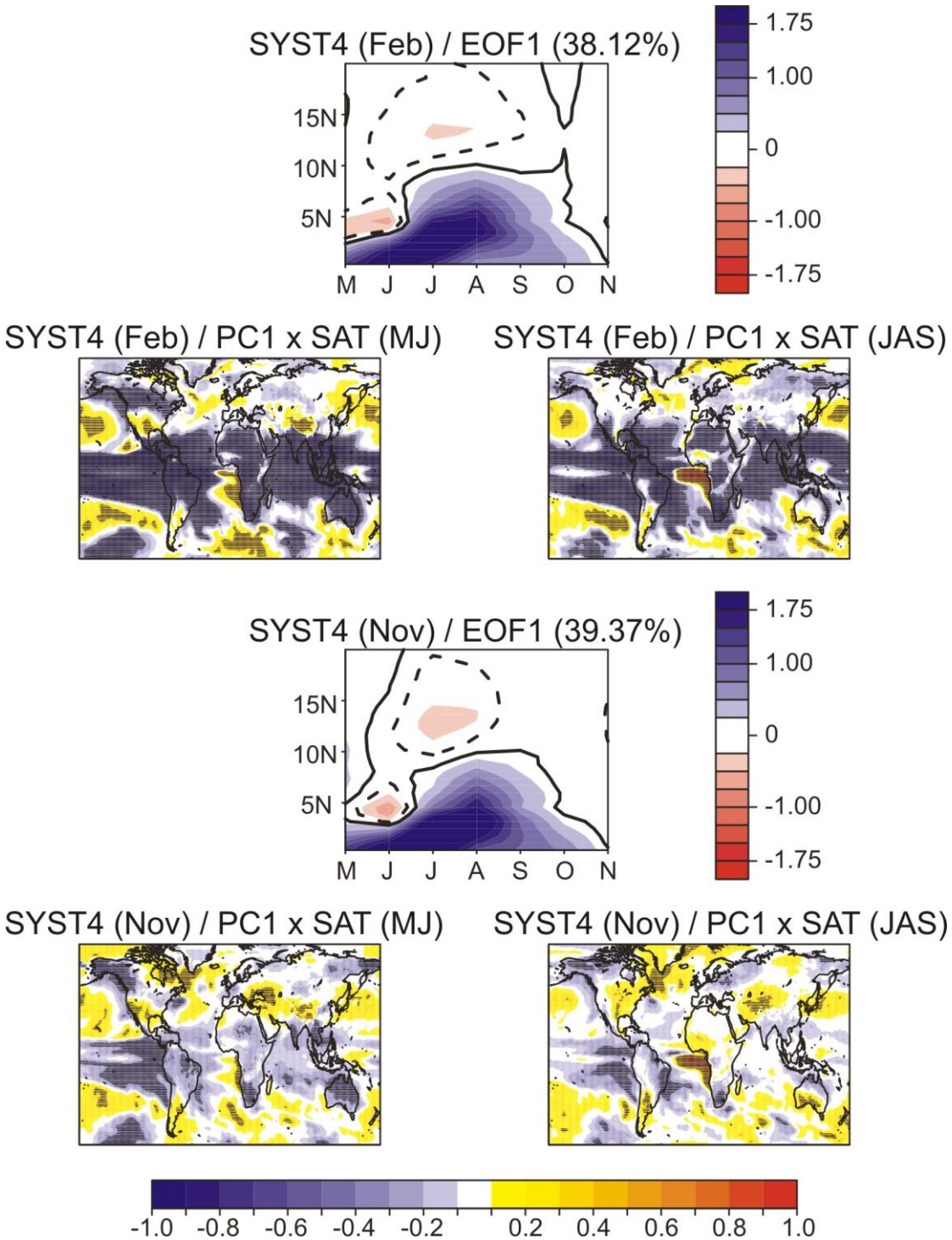

Figure 5. Same as Fig. 3, but for the other two start dates considered: February (3-month lead time), and November (6-month lead time).

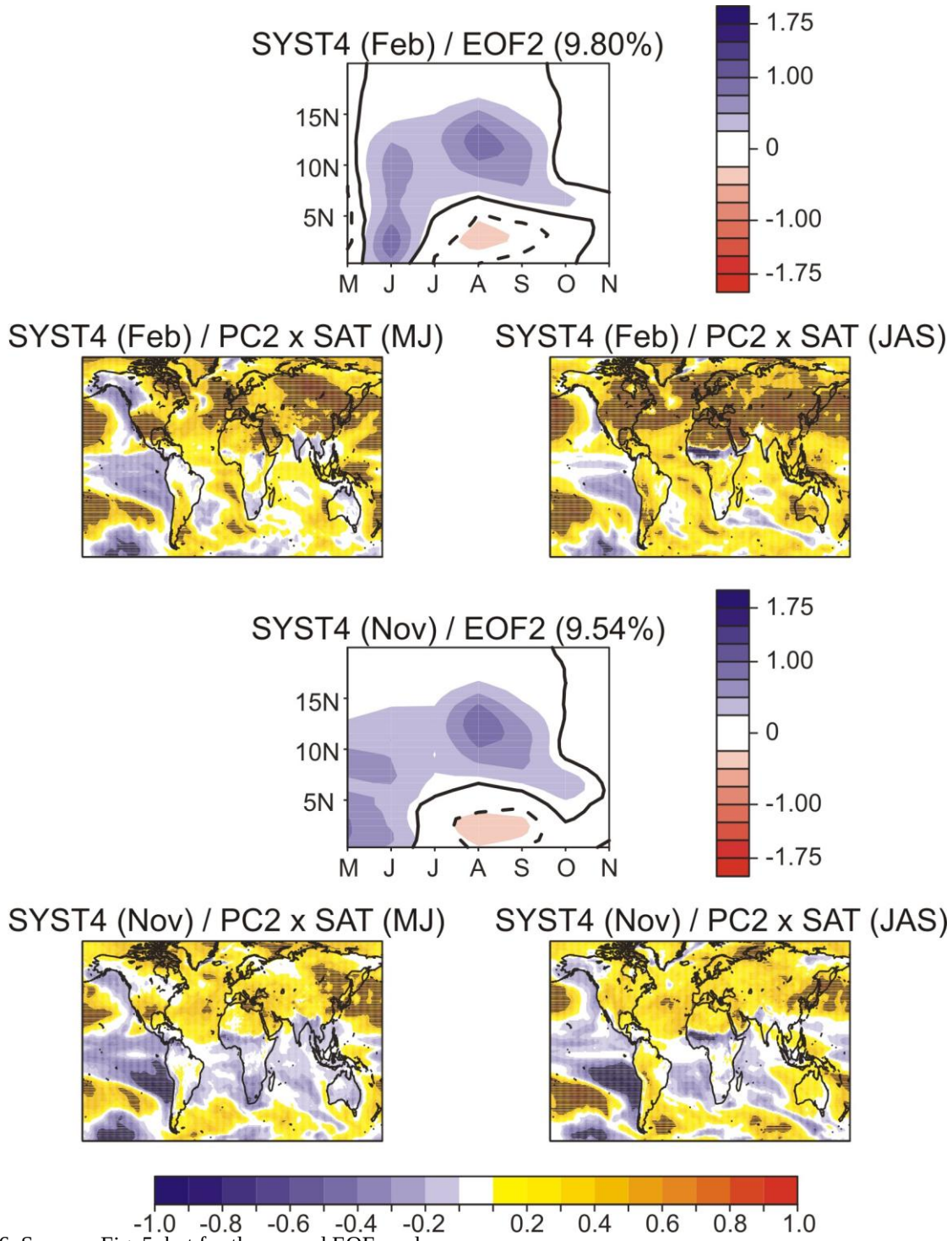

Figure 6. Same as Fig. 5, but for the second EOF mode.

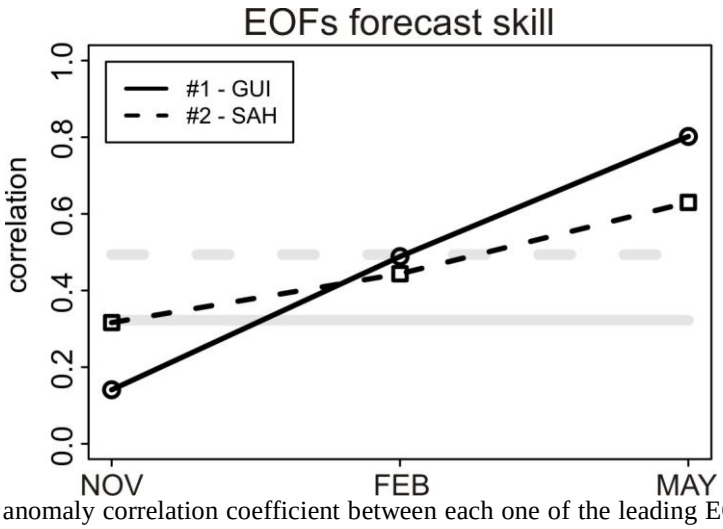

Figure 7. Ensemble-mean anomaly correlation coefficient between each one of the leading EOFs of the longitudinally-averaged precipitation over West Africa in ECMWF-System4 and GPCP; Guinean (first mode; solid) and Sahelian (second mode; dashed) rainfall regimes. Confidence levels (α<0.05, one-tailed *t*-test) for positive, different from zero correlations are drawn as horizontal grey lines; the effective number of degrees of freedom has been computed separately from the observed EOF1 (Guinean regime) and EOF2 (Sahelian regime).

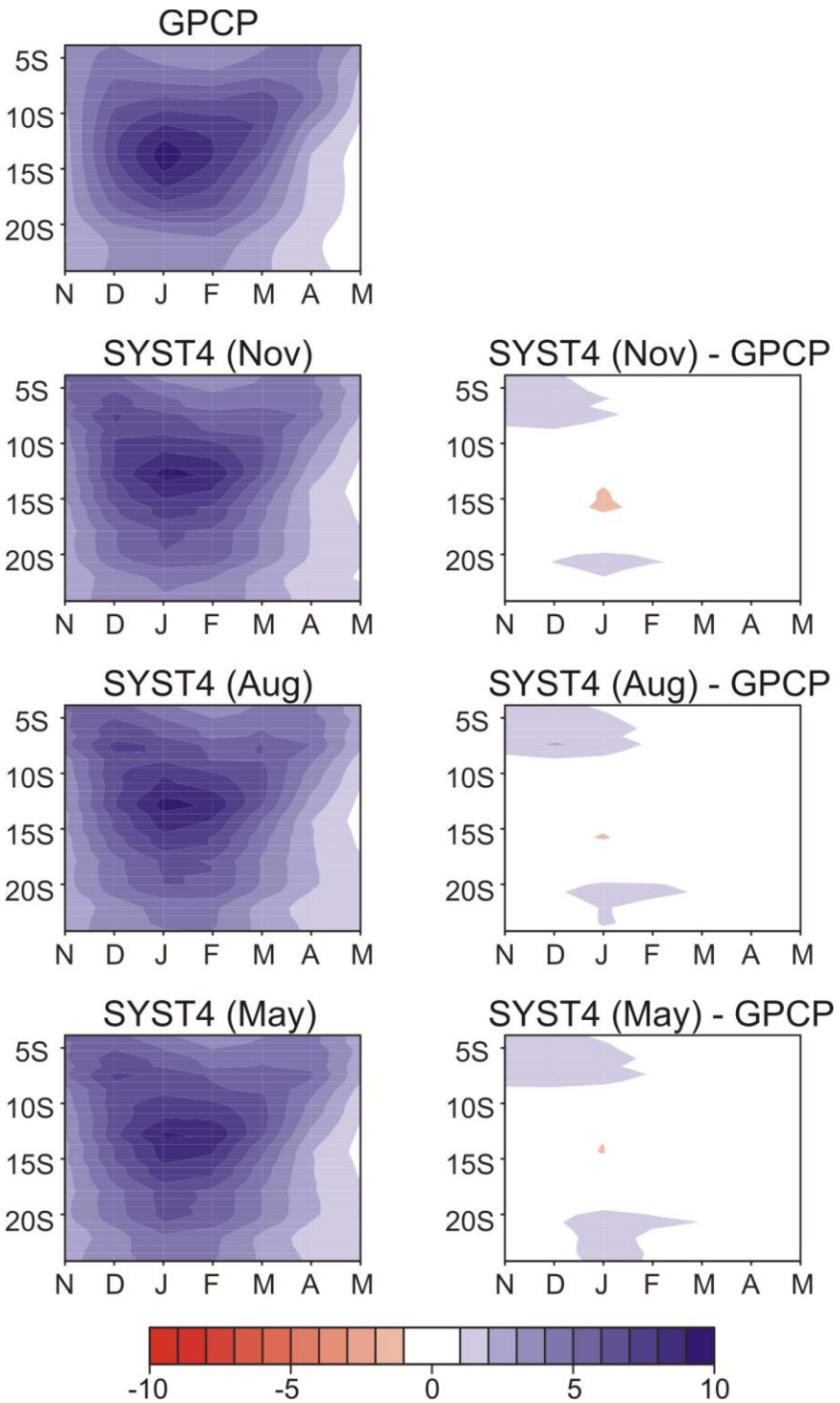

Figure 8. Hovmöller latitude-time diagrams of eastern South African (see Fig. 1) precipitation climatology (mm/day) for GPCP (top-left) and ECMWF-System4 (left column), and the differences between them (right column). The three start dates considered in this case are: November (zero lead time; solid black), August (3-month lead time; dashed black), and May (6-month lead time; dotted black). Period of study for the Hovmöller diagram is 1982-2008.

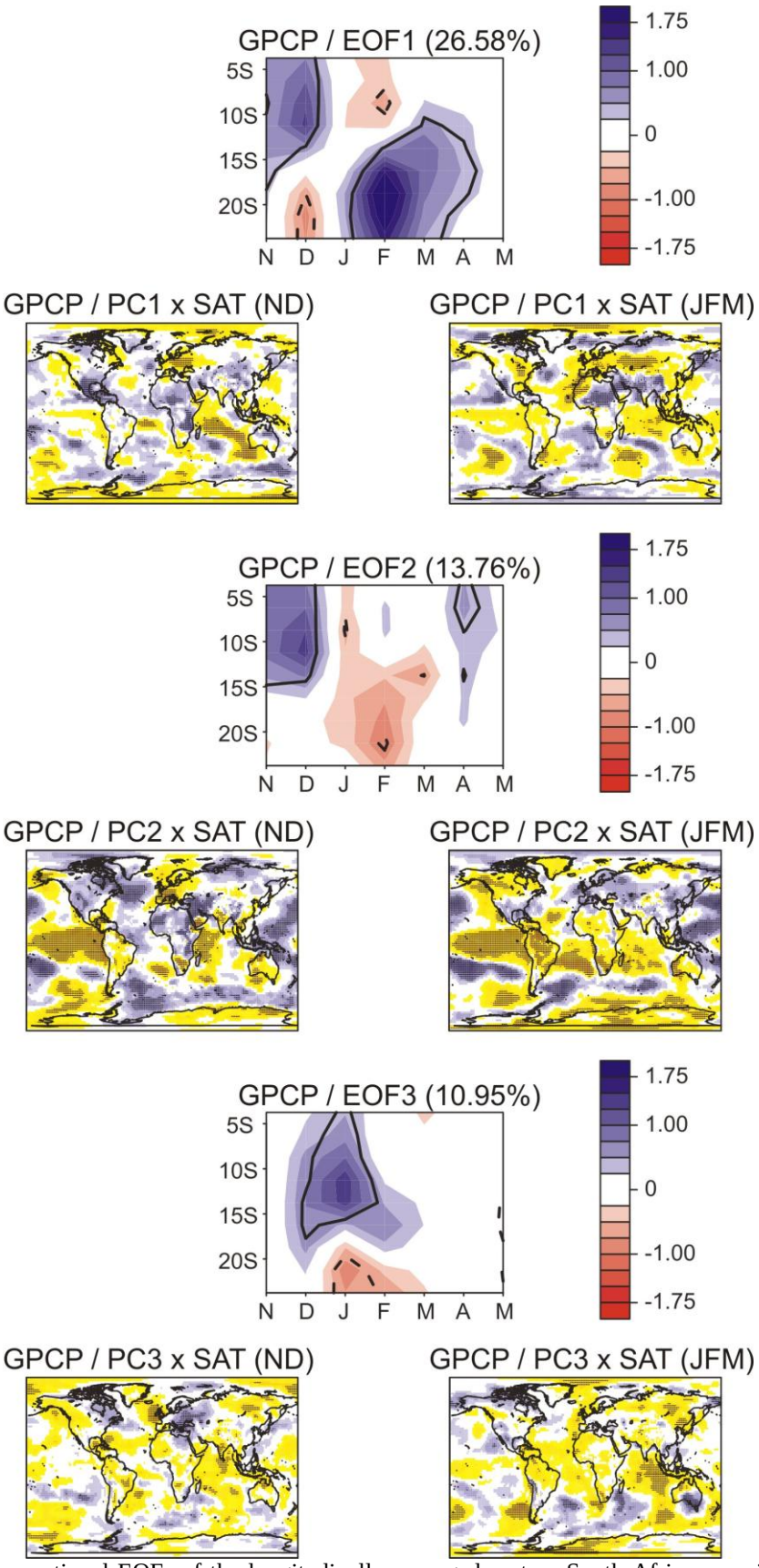

Figure 9. Leading observational EOFs of the longitudinally-averaged eastern South African precipitation (30ºE-40ºE) over the period 1982-2008; and associated correlation maps of the principal component onto the surface air temperature (NCEP/NCAR) for austral early-summer (November-December) and late-summer (January-March).

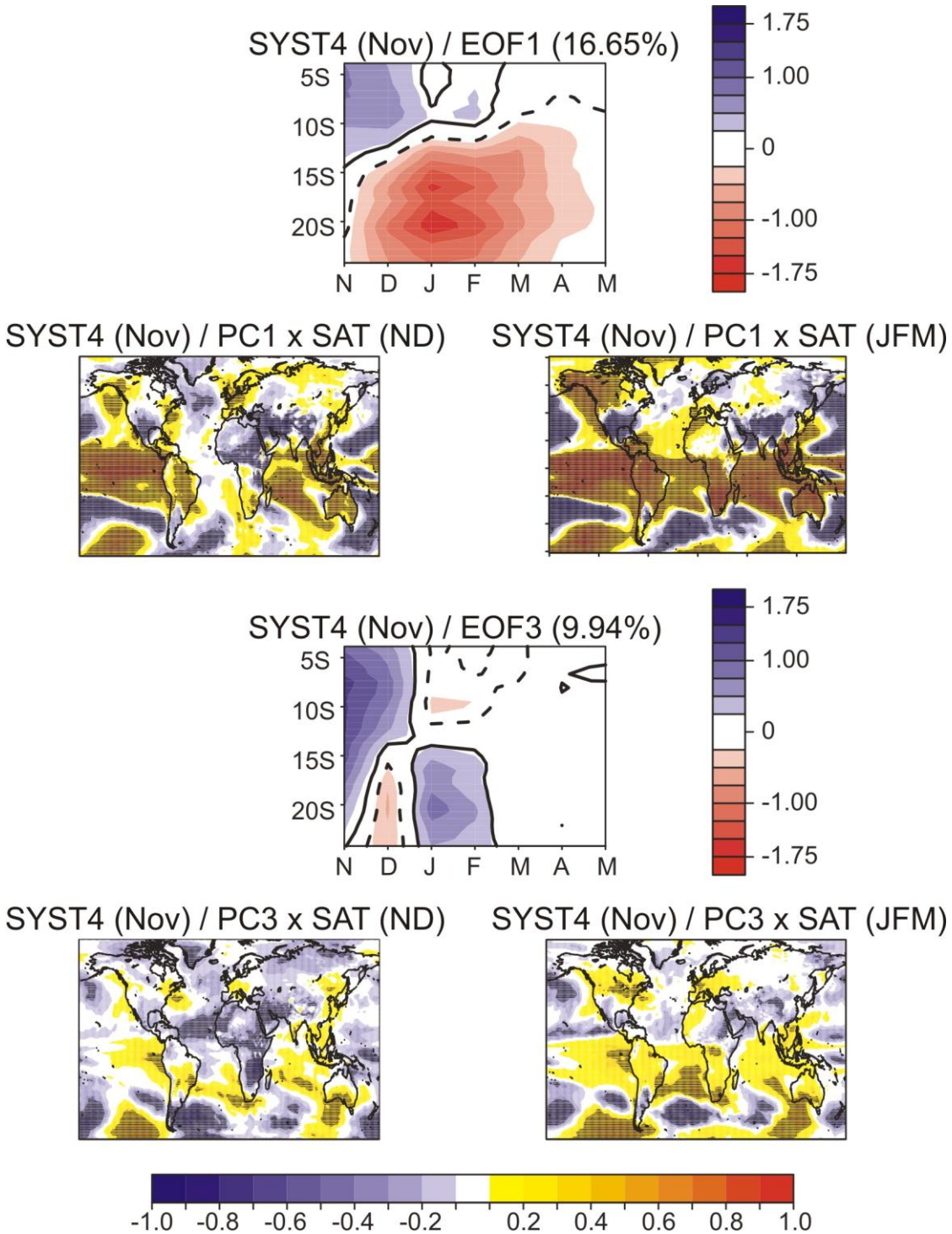

Figure 10. (top) First and (botom) third leading EOFs of the longitudinally-averaged eastern South African precipitation (30ºE-40ºE) and associated correlation maps of the principal component onto the surface air temperature for austral early-summer (November-December) and late-summer (January-March) in the ECMWF-System4 seasonal/annual hindcasts for the start date of November. The principal component analysis was carried out by considering all the members in the co-variance matrix (Philippon et al. 2010).